Mon. Not. R. Astron. Soc. **270,** 325–340 (1994)

Observations and dynamical modelling of the E4 galaxy NGC 2974: evidence for an embedded stellar disc

Pierantonio Cinzano[1] and Roeland P. van der Marel[2]★

[1] *Dipartimento di Astronomia, Università di Padova, 35122 Padova, Italy*
[2] *Sterrewacht Leiden, Postbus 9513, 2300 RA Leiden, The Netherlands*

Accepted 1994 April 19. Received 1994 April 15; in original form 1994 January 24

ABSTRACT

It has recently been realized that some, and possibly very many, galaxies classified as elliptical might contain an embedded stellar disc. Here we present a case study: NGC 2974, classified as E4. Discs of dust, neutral gas (H I) and ionized gas (Hα) have all been detected in this galaxy. The observed stellar rotation is much higher than in typical elliptical galaxies, $(V/\sigma)^* \approx 1.5$, and the isophotes are slightly pointed.

We present new long-slit spectroscopic data along the major, the minor and an intermediate axis of NGC 2974. From these data, we determine rotation velocities, velocity dispersions and deviations of the velocity profiles from a Gaussian, as quantified by the Gauss–Hermite moments h_3 and h_4. On the major axis, the velocity profiles are asymmetric, with the asymmetry changing sign upon going from one side of the nucleus to the other.

We construct detailed dynamical models consisting of an axisymmetric bulge and a thin exponential disc. We study disc–bulge combinations that fit the observed surface brightness, ellipticity and a_4 profiles, and solve the equations of hydrostatic equilibrium for the disc and the bulge in the total potential of the system. The predicted kinematics and velocity profile shapes are compared with the data. To fit the observed ratio of major to minor axis rms motion without invoking the presence of a stellar disc requires the galaxy to have an intrinsic axial ratio $q_t \lesssim 0.25$. This is unrealistically flat: elliptical galaxies with apparent flattening $q_a \lesssim 0.3$ are never observed. An acceptable fit to all the available photometrical and kinematical data is obtained with a model inclined at $\sim 57°.5$ that has an embedded stellar disc that contains ~ 7 per cent of the total light of the galaxy. The disc has $V/\sigma \gtrsim 3$ and is thus rotationally supported. At a larger inclination angle, NGC 2974 would presumably have been classified as an S0.

We model the ionized gas kinematics of NGC 2974 presented by Amico et al. and Zeilinger et al. by assuming the gas to consist of individual clumps that orbit as test particles in the potential defined by the bulge and the embedded stellar disc. The model provides an excellent fit to the observed streaming velocities of the ionized gas, indicating that these are consistent with the potential derived from the stellar kinematics, and the asymmetric drift implied by the observed non-zero velocity dispersion of the gas. The kinematics of the stellar disc and the ionized gas disc are very similar, suggestive of a common evolutionary history.

The total luminous mass of NGC 2974 is $M_{\rm lum} = 2.4 \times 10^{11}\ h_{50}^{-1}\ {\rm M}_\odot$. The H I data presented by Kim et al. indicate that NGC 2974 has a dark halo with $M_{\rm halo}(<3.6R_e) = 3.6 \times 10^{11}\ h_{50}^{-1}\ {\rm M}_\odot$. In the region of our spectroscopic data ($\lesssim 0.5R_e$) the dynamical influence of the dark halo is negligible.

Key words: line: profiles – galaxies: elliptical and lenticular, cD – galaxies: individual: NGC 2974 – galaxies: kinematics and dynamics – galaxies: photometry – galaxies: structure.

★Present address: Institute for Advanced Study, Princeton, NJ 08590, USA.

1 INTRODUCTION

The morphological class of elliptical galaxies contains objects with different physical properties. A useful observational subdivision is made according to isophote shape: some elliptical galaxies have 'pointed' or 'discy' isophotes, others have 'boxy' isophotes. Striking relations exist between isophote shapes and the dynamical, radio and X-ray characteristics of elliptical galaxies (e.g. Bender 1990a). The pointedness of the isophotes could be the result of the presence of an embedded stellar disc (e.g. Carter 1987; Capaccioli 1987). This would naturally explain the fact that discy galaxies tend to rotate more rapidly than boxy galaxies (Bender 1988). Rix & White (1990) demonstrate that the presently available data even allow the possibility that *all* non-boxy elliptical galaxies have embedded stellar discs, because in galaxies that are not close to edge-on such discs are very hard to detect. On the other hand, discy isophotes do not necessarily imply the presence of a stellar disc. One-component mass models in axisymmetric or triaxial potentials can also produce shapes with pointed isophotes (e.g. Miyamoto & Nagai 1975; de Zeeuw, Franx & Peletier 1986). Some simulations of dissipationless collapse result in structures that appear discy if seen from one orientation and boxy if seen from another (Stiavelli, Londrillo & Messina 1991). Remnants of galaxy mergers can also have discy isophotes (e.g Governato, Reduzzi & Rampazzo 1993). It is clearly important to improve our understanding of elliptical galaxies with embedded discs. To date, we do not know how common these galaxies are, nor do we know whether they form a physically distinct class from either normal ellipticals, normal S0s, or both. Also, the presence of embedded discs may be a significant source of scatter in the fundamental plane relation for elliptical galaxies.

Searching for elliptical galaxies with embedded discs is difficult by definition, given that all ellipticals with obvious discs have been classified as S0s. One way to detect a weak disc in an elliptical galaxy is to do a disc–bulge decomposition of the observed photometry. This decomposition is generally non-unique, and additional assumptions must be made. It is often assumed either that the isophotes of the bulge are perfectly elliptical (e.g. Scorza & Bender 1990) or that the disc has an exponential surface-brightness profile. Neither of these assumptions necessarily has to be true. For a review of existing methods, see Capaccioli & Caon (1992). The arguments for an embedded stellar disc can be strengthened considerably by modelling also the observed kinematics. An embedded stellar disc will enhance the observed rotation velocities. In addition, the stellar line-of-sight *velocity profiles* (VPs, hereafter) will deviate from a Gaussian. On the major axis the VPs will be asymmetric, with the asymmetry changing upon going from one side of the nucleus to the other (Franx & Illingworth 1988; Bender 1990b; Rix & White 1992).

Two elliptical galaxies for which the presence of an embedded stellar disc has been established from photometric and kinematic data are NGC 3610 (Scorza & Bender 1990; Rix & White 1992) and NGC 5322 (Bender, Döbereiner & Möllenhoff 1988; Bender 1990a; Rix & White 1992). NGC 3610 has very pointed isophotes, $a_{4,\max} \approx 0.03$, and rotates faster than an oblate isotropic rotator, $(V/\sigma)^* \approx 1.1$. Modelling of the data indicates that NGC 3610 is close to edge-on, $i = 80°$, and contains an embedded stellar disc that contributes ~ 7 per cent of the total luminosity. The disc has $V/\sigma \approx 4.5$, and is supported by rotation. NGC 5322 has discy isophotes in the inner 7 arcsec, $a_{4,\max} \approx 0.01$, but is boxy in the outer parts. It has a counter-rotating core. Modelling of the data yields an inclination $i = 68°$ and an embedded stellar disc that contains ~ 13 per cent of the light in the inner 12 arcsec. The disc has $V/\sigma = 1.3$ and is thus largely pressure-supported.

Here we present a detailed study of the galaxy NGC 2974. Preliminary results from this project were discussed in Cinzano & van der Marel (1993). A related discussion of the same galaxy was given by Scorza (1993b). NGC 2974 is classified E4 in both the RSA (Sandage & Tammann 1981) and the RC3 (de Vaucouleurs et al. 1991). It has slightly pointed isophotes (Bender et al. 1988; Nieto et al. 1991), and rotates rapidly. Its $(V/\sigma)^* \approx 1.5$ (Bender 1988) sets it well above the curve for rotationally flattened objects in the V/σ versus ε diagram. This suggests that NGC 2974 might have an embedded stellar disc. H I 21-cm observations have detected neutral gas in a flat structure well aligned with the optical isophotes (Kim et al. 1988). The zero-velocity curve of the H I velocity field is well aligned with the optical minor axis. This is consistent with a rotating H I disc with inclination $i \approx 55°$. Ionized gas has also been detected. Hα images (Buson et al. 1993) show that it is distributed in a flat structure along the major axis. If distributed in a disc, the ellipticity implies that $i \approx 59°$. Modelling of the kinematics of the ionized gas yields $i \approx 55°$ (Amico et al. 1993). Outside ~ 5 arcsec, the distribution of the ionized gas becomes filamentary, reminiscent of the appearance of an Sa galaxy. In fact, similar filamentary and 'arm-like' structures can be seen on deep optical images (Schweizer, private communication; Buson et al. 1993). A $B-R$ image (Kim 1989) shows a flat structure aligned with the major axis, presumably caused by reddening due to dust. The flattening of the $B-R$ contours suggests that $i \approx 60°$. Molecular gas has been searched for in the CO (1-0) transition, but was not detected (Bregman, Hogg & Roberts 1992).

We present new spectroscopic data for NGC 2974 and derive the kinematics and VP shapes. We construct detailed dynamical models to interpret the results. We solve the Jeans equations for both the disc and the bulge in the total potential of the system. By enforcing hydrostatic equilibrium, the freedom in the interpretation of the data is substantially reduced. To date, only for NGC 5322 have simple arguments been presented that the detected disc is actually in hydrostatic equilibrium in the potential of the system (Rix & White 1992).

In Section 2, we present the spectroscopic data and the kinematic and VP analysis. In Section 3, we discuss photometry of NGC 2974. The dynamical modelling technique is discussed in Section 4, and is used to interpret the data in Section 5. Conclusions are presented in Section 6.

2 SPECTROSCOPIC DATA AND VELOCITY PROFILE ANALYSIS

2.1 Observations and data reduction

Long-slit spectra of NGC 2974 were obtained with the Boller and Chivens spectrograph equipped with the CCD

number 8, mounted at the Cassegrain focus of the ESO 3.6-m telescope at La Silla, Chile. These spectra were taken as part of a larger project in collaboration with F. Bertola, I. J. Danziger, P. T. de Zeeuw and W. W. Zeilinger. Slits were aligned along the major axis (PA=225°), the minor axis (PA=315°) and an intermediate axis (PA=270°). The exposure times were 90, 90 and 45 min, respectively. The major and minor axis data consist of two separate 45-min exposures that were reduced separately, and added later. The spectra were rebinned at the telescope over 3 pixels in the spatial direction, giving a scale of 1.65 arcsec pixel^{-1}. The seeing during the observations, determined as described in Section 4.3, was ~1.9 arcsec FWHM. The 1200 line mm^{-1} ESO number 26 grating was used, giving a dispersion of 0.89 Å pixel^{-1}. The spectra covered the range from 4750 to 5600 Å, centred on the Mg *b* triplet (~5175 Å). A slit width of 1.51 arcsec was used, resulting in an instrumental velocity resolution of 45 km s^{-1} (Gaussian dispersion of the lines in arc lamp spectra). Spectra of G and K giants were taken for use as templates. Stellar spectra were reduced similarly to the galaxy spectra, and averaged along columns to yield one spectrum of high signal-to-noise ratio (S/N) for each star. The reduction of the frames was standard and was done with the ESO MIDAS package. After bias and dark current subtraction, frames were flat-fielded and cleaned from cosmic rays and CCD defects. Wavelength calibration was done using He–Ar arc lamp spectra. Sky subtraction was done using the available data at the ends of the slit. Where necessary, galaxy spectra were rebinned in the spatial direction to increase the S/N. Emission lines of [O III]4959 Å, [O III]5007 Å and [N I]5200 Å were interpolated over.

2.2 Velocity profile analysis

The spectra were analysed with the Fourier Fitting Method, as described by Franx, Illingworth & Heckman (1989), and later modified by van der Marel & Franx (1993, hereafter vdMF) to allow determination of deviations of the VP from a Gaussian. The galaxy spectrum is assumed to be the convolution of a template spectrum and the VP. The VP is expanded about a Gaussian in a sum of orthogonal functions: the Gauss–Hermite series. This approach was proposed independently by vdMF and Gerhard (1993). Following vdMF, we write the VP as

$$\mathscr{L}(v)=[\gamma\alpha(w)/\sigma]\left[1+\sum_{j=3}^{4} h_j H_j(w)\right],$$

$$w\equiv(v-V)/\sigma, \qquad \alpha(w)=\frac{1}{\sqrt{2\pi}}\,\mathrm{e}^{-w^2/2}, \tag{1}$$

where v is the line-of-sight velocity. The functions $H_l(y)$ are the *Hermite polynomials* given in Appendix A of vdMF. The first term of the series represents a Gaussian VP with line strength γ, mean radial velocity V and velocity dispersion σ. The coefficient h_3 measures the lowest order antisymmetric deviation from a Gaussian. If h_3 has the opposite sign to V, there is a tail of stars away from the direction of rotation. The coefficient h_4 measures the lowest order symmetric deviation. A positive value of h_4 usually indicates that the VP is more centrally peaked than a Gaussian, a negative value that it is more flat-topped.

If γ_0 is the true difference in line strength between the galaxy and template spectra and $\mathscr{L}_0(v)$ is the true normalized VP, then, for 'ideal data' (no noise, continuum subtraction and template mismatching, etc.) and given (γ, V, σ), the best-fitting h_l are the *Gauss–Hermite moments*,

$$h_l=(2\sqrt{\pi})\,\frac{\gamma_0}{\gamma}\int_{-\infty}^{\infty}\mathscr{L}_0(v)\,\alpha(w)\,H_l(w)\,\mathrm{d}v. \tag{2}$$

In practice, the parameters of the VP are determined by χ^2 fitting in Fourier space of the broadened template spectrum to the galaxy spectrum. Both a high- and a low-wavenumber cut-off are used, the former motivated by the finite spectral resolution of the instrument, the latter to discard the low-frequency information that remains after continuum subtraction. To obtain parameters (γ, V, σ) from the data, one can (a) fit a Gaussian VP to the data; or (b) fit the parametrization (1) to the data. The results of these two methods are (virtually) identical, due to the orthogonality of the Gauss–Hermite series (as described in vdMF). We have used method (a), because this requires less rebinning of the data in the spatial direction. The parameters (h_3, h_4) were obtained with method (b). In principle, it does not matter how one determines the parameters of the VP, as long as one treats the model VPs and the observed VPs similarly. This is indeed what we do in Sections 4 and 5.

The K0III star HD 2035 was used as a template. No attempt was made to construct an optimal template by combining the spectra of stars of different stellar types, as was done by Rix & White (1992) and van der Marel et al (1994a). As a result, we cannot exclude the possibility of systematic errors in our Gauss–Hermite moments, but these errors are expected to be small, $|\Delta h_l| \lesssim 0.03$ (vdMF).

2.3 Results

The (V, σ, h_3, h_4) obtained from the VP analysis are plotted in Fig. 1. For the intermediate axis data, h_3 and h_4 could not be determined because of low S/N. Before plotting, results at negative radii were folded to positive radii (results for V and h_3 at negative radii were multiplied by -1 because these quantities should be odd functions of radius along the slit). Results from positive and negative radii generally agree well.

The amplitude of the major axis rotation curve is ~215 km s^{-1}, unusually high for an elliptical galaxy. No minor axis rotation is detected. The velocity dispersion has a maximum of ~225 km s^{-1} in the centre. The major axis σ profile has a minimum of ~110 km s^{-1} at ~11 arcsec. At ~13 arcsec, the ratio v of the projected rms velocity $\sqrt{V^2+\sigma^2}$ on the major and minor axes is as large as ~1.85. This indicates that the amount of rms motion on the major axis of NGC 2974 is truly unusual. For a sample of 37 elliptical galaxies studied by van der Marel (1991), v was always $\lesssim 1.4$.

The VPs on the major axis are asymmetric, as measured by the non-zero value of h_3. The sign of the asymmetry changes upon going from one side of the nucleus to the other. This is what would be expected if an embedded stellar disc were present. The quantity h_4 tends to increase with increasing galactocentric distance, on both the major and the minor axes. The solid curves in Fig. 2 show the major axis VPs of NGC 2974 at different radii along the slit. For this plot, data

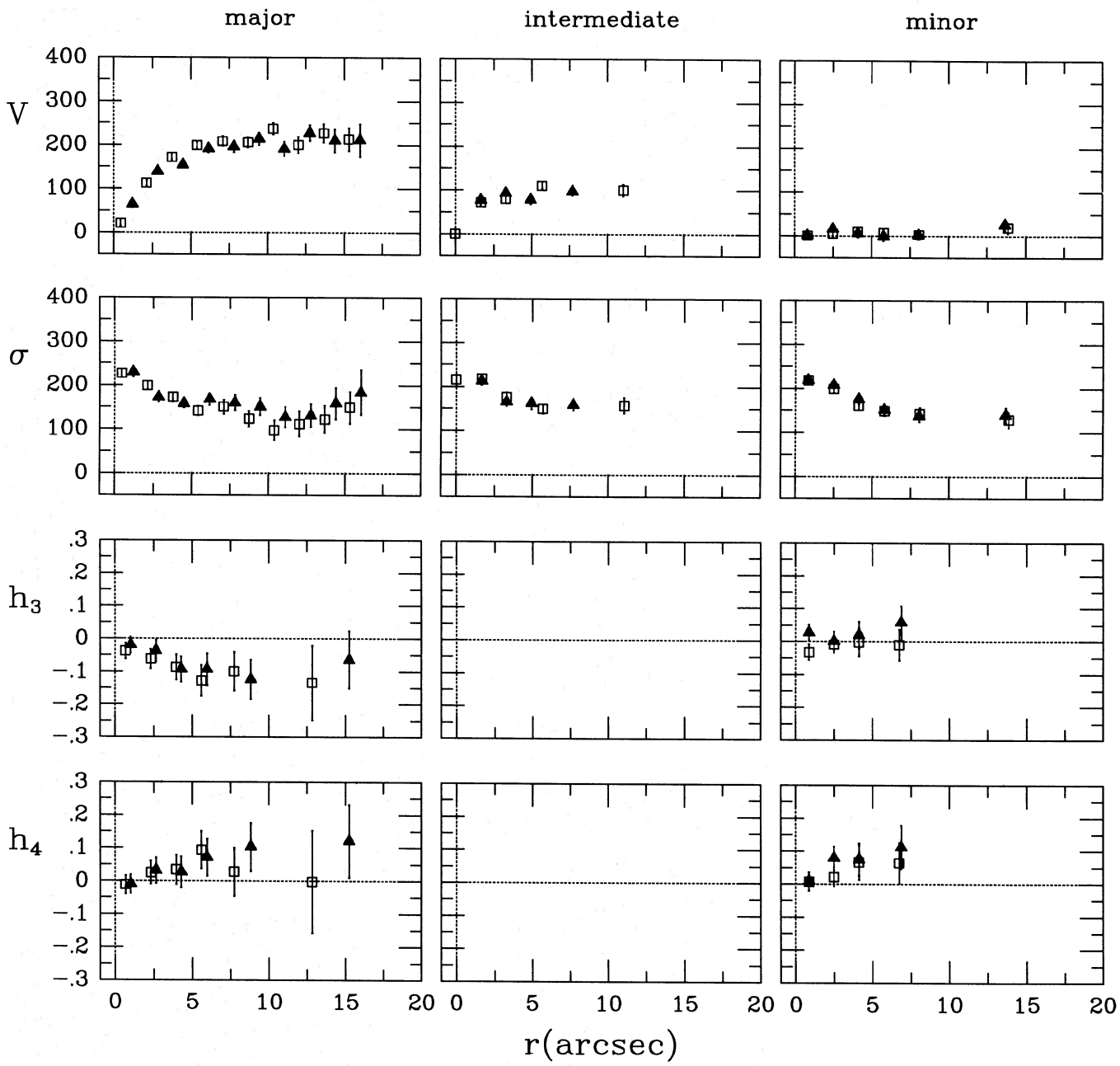

Figure 1. Shown for the major, intermediate and minor axes of NGC 2974 are, from top to bottom, rotational velocities, velocity dispersions, and the VP shape coefficients h_3 and h_4, determined as described in the text. The coefficient h_3 measures antisymmetric deviations of the VP from a Gaussian, while h_4 measures symmetric deviations. Solid symbols denote results from positive radii, open symbols denote folded results from negative radii. Positive radii lie towards the east. Velocities are in km s^{-1}. The quantities h_3 and h_4 could not be determined for the intermediate axis, due to the low signal-to-noise ratio of these data.

at positive and negative radii were averaged, assuming the VPs to be reflection symmetric at diametrically opposed points in the galaxy. The asymmetry of the VPs is clearly visible.

2.4 Double Gaussian decomposition

The advantage of using h_3 and h_4 to describe deviations of the VP from a Gaussian is that the errors in these parameters are uncorrelated, and that the parameters themselves are always well defined. This is not true for a double Gaussian decomposition of the VP (a fit of the sum of two Gaussians to the data), which has been used in studies of other galaxies (e.g. Franx & Illingworth 1988; Bender 1990a; Rix & White 1992). Such a decomposition is ill-defined if, for example, the second component contributes only little light, or if both components have comparable rotational velocities. This complicates the VP analysis close to the centre and on the minor axis.

On the other hand, we do have reason to suspect that there might be two kinematically distinct components present in NGC 2974. Double Gaussian decompositions of

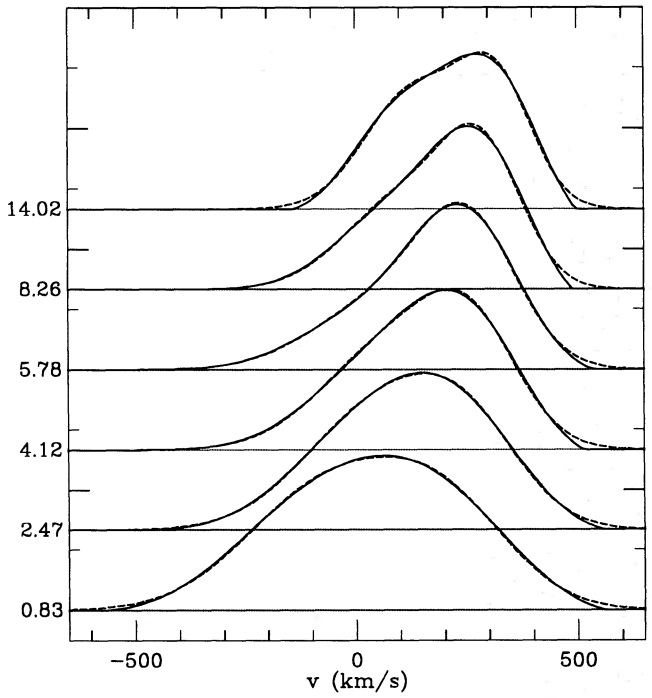

Figure 2. VPs for the major axis of NGC 2974 at different radii along the slit (as listed in the left margin of the plot). Solid curves are the Gauss–Hermite series fits to the data (set to zero in the wings when the parametrization implies a negative value). The dashed curves are the best double Gaussian fits to the solid curves. The normalization is arbitrary.

the VPs thus do seem useful, as they yield rough estimates of the characteristics of the different components. We therefore fitted double Gaussians (dashed curves in Fig. 2) to the major axis VPs obtained with the Fourier Fitting Method (solid curves in Fig. 2). In the wings there are some systematic differences between the solid and dashed curves, but the wings are not particularly well determined by the data anyway (because of inaccuracies in the continuum subtraction stage). A direct fit of double Gaussians to the data, kindly provided by Hans-Walter Rix, and obtained with the method described in Rix & White (1992), yielded similar results to those from our approach.

Fig. 3 displays the parameters of the double Gaussian fits displayed in Fig. 2. The systematic errors in these parameters can be large (easily 20 per cent), given that the parameters of a double Gaussian fit are highly correlated (different combinations of parameters can give very similar VPs). The results for the innermost VP ($r = 0.83$ arcsec) are omitted from Fig. 3. This VP is close to Gaussian, and the parameters of the double Gaussian fit to this VP are thus particularly ill-determined.

We refer to the most rapidly rotating component in the double Gaussian decomposition as the 'disc', and to the other component as the 'bulge' (even though it is not a priori clear whether the two components are indeed a disc and a bulge). The disc rotates with an amplitude of ~ 280 km s^{-1}, the bulge with an amplitude of ~ 120 km s^{-1}. In the inner 15 arcsec, the dispersion of the bulge falls from ~ 180 km s^{-1} to ~ 110 km s^{-1}, and that of the disc from ~ 140 km s^{-1} to ~ 80 km s^{-1}. The disc has $V/\sigma \gtrsim 3$. The fraction of the light contributed by the disc component, $f_{\rm disc}$, is between 30 and 60 per cent. The bottom right panel in Fig. 3 displays the natural logarithm of the intensity of the disc component along the slit (as obtained by multiplying the observed total intensity with $f_{\rm disc}$). The dashed line in this panel is the best linear least-squares fit, and corresponds to an exponential surface-brightness profile with scalelength $R_{\rm d} = 6.0$ arcsec.

The results of single Gaussian and double Gaussian VP fits to the data should both be interpreted with care. Continuum subtraction and Fourier filtering remove low-wavenumber information from the galaxy spectrum. If two kinematically distinct components are present in the galaxy, the high-dispersion component is more influenced by this than the low-dispersion component. As a result, the dispersion of the best-fitting Gaussian VP to the data is an underestimate of the true line-of-sight velocity dispersion (McElroy 1983). Similarly, a double Gaussian VP fit is likely to overestimate the fraction of the light contributed by the low-dispersion component. It is therefore best to regard the parameters derived here as fitting parameters, rather than as determinations of physical quantities. When modelling the data in Sections 4 and 5, we take the effects of low Fourier wavenumber filtering into account.

3 PHOTOMETRIC DATA

3.1 Surface brightness and isophote fitting

In order to model NGC 2974 we also need photometry, in addition to spectroscopy. We analysed an image kindly placed at our disposal by Lucio Buson, which has been previously discussed by Buson et al. (1993). The image was obtained by John Danziger, with the ESO 2.2-m telescope with the ESO number 390 filter, in the continuum near Hα. It is an average of two 1080-s exposures, taken with seeing of ~ 1.1 arcsec FWHM and binned 2×2 to give a scale of 0.352 arcsec pixel^{-1}. We analysed the image using the 'Astronomical Images Analysis Package' running on the VAX 4000/500 at the Dipartimento di Astronomia in Padova (Fasano 1990). Intensities on our image were converted to Johnson's R band by scaling the image to a 900-s R-band image obtained at the Asiago-Ekar 1.82-m telescope with the Tektronics TK512M CCD and calibrated with Landolt (1983) photometric standard stars. (If required, these intensities, and also the mass-to-light ratios to be derived below, can be transformed to Cousins' R band by using the relations given by Peletier et al. 1990.) The surface brightness, ellipticity and a_4 profiles thus obtained are displayed in Fig. 4.

Our major axis surface-brightness profile agrees well with those of Djorgovski (1985) and Buson et al. (1993). Between 5 and 64 arcsec, it is well fitted by an $R^{1/4}$ law with effective radius $R_{\rm e} = 33.7$ arcsec and effective R-band surface brightness $m_{\rm e} = 20.5$ mag arcsec^{-2}. Assuming a mean axial ratio of 0.64, this implies a total apparent R-band magnitude of $R_{\rm T} = 9.96$. The total apparent B-band magnitude is $B_{\rm T} = 11.87$ (RC3). This implies that $B - R = 1.91$, a typical value for elliptical galaxies (Peletier et al. 1990). Henceforth we assume that $H_0 = 50$ km s^{-1} Mpc^{-1}. The distance to NGC 2974 is then 38.5 Mpc, based on the observed heliocentric velocity of 1924 km s^{-1} (Davies et al. 1987). At this

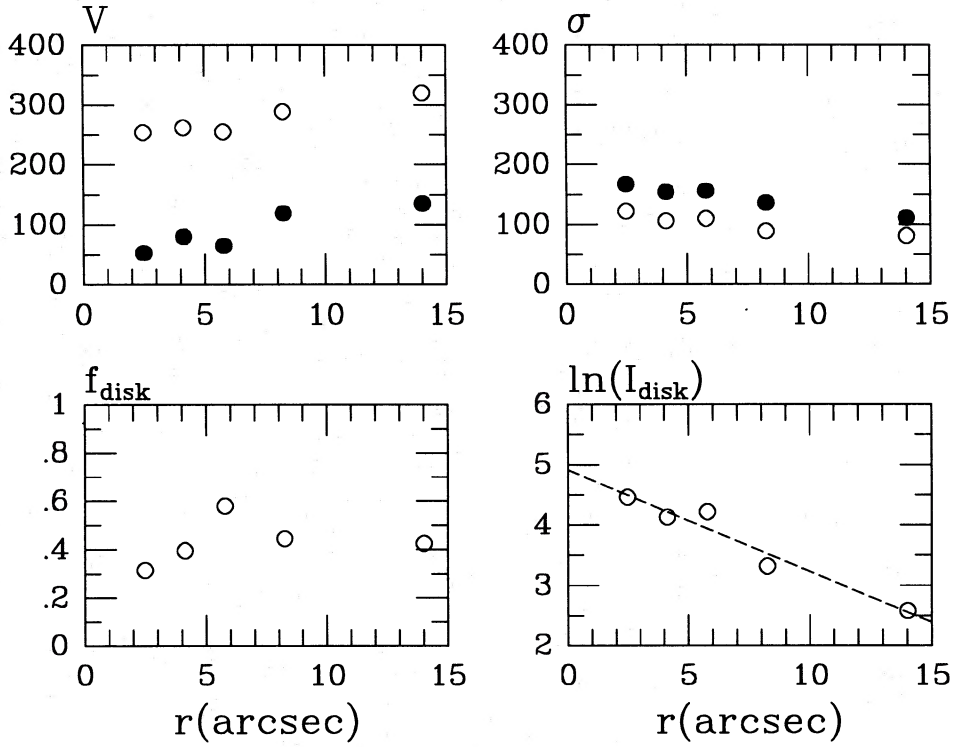

Figure 3. Parameters of the double Gaussian fits plotted in Fig. 2. The top panels show the rotation and dispersion of the disc (open symbols) and bulge (solid symbols) components. The bottom left panel shows the fraction of the light contributed by the disc component. The bottom right panel shows the natural logarithm of the intensity of the disc component along the slit. The dashed line is the best-fitting exponential surface-brightness profile. It has scalelength $R_d = 6.0$ arcsec.

distance, 1 arcsec corresponds to 0.187 h_{50}^{-1} kpc. The total R-band luminosity of the galaxy is $8.1 \times 10^{10}\ h_{50}^{-2}\ L_\odot$ and the total B-band luminosity is $4.1 \times 10^{10}\ h_{50}^{-2}\ L_\odot$.

The a_4 coefficient measures the Fourier component $\delta I = a_4 \cos\theta$ of the intensity variations along the best-fitting ellipse to an isophote. The a_4 coefficient is positive, as already demonstrated by Bender et al. (1988), Nieto et al. (1991) and Buson et al. (1993). This implies that the isophotes are discy. The maximum in a_4 occurs at $R \approx 12$ arcsec. Taking into account differences in the definitions of a_4, our results agree well with those of previous authors. There are some differences with the I-band results presented by Bender et al., but this is presumably due to the presence of dust.

3.2 Photometric disc–bulge decomposition

Even though the positive value of the a_4 coefficient hints at the presence of a disc, a photometric disc–bulge decomposition is not straightforward. The a_4 coefficient is not large and the observations of neutral and ionized gas in NGC 2974 suggest that the disc is not close to edge-on. The presence of dust makes the interpretation of higher order Fourier coefficients, such as a_6, difficult. The surface-brightness profile of the bulge component is not known a priori, and an $R^{1/4}$ law is not necessarily a good representation (Burstein 1979; Simien & Michard 1984; Capaccioli 1987, 1990). Also, the disc surface-brightness profile is not necessarily well described by an exponential (Scorza 1993a). One could assume that the bulge has perfectly elliptical isophotes (Scorza & Bender 1990) or constant ellipticity, but there is no physical reason why this should always be so.

None the less, we tried a number of different approaches of obtaining a photometric disc–bulge decomposition for NGC 2974, but only with the aim of obtaining rough bounds on the parameters of the disc. We do not attempt to model the influence of dust on the measured isophote shapes, even though this does deserve further study.

First, we masked part of the galaxy image with a 'butterfly' mask and analysed the remaining part of the isphotes. (In doing so, we used the same ellipse-fitting software as before, but excluded masked pixels from the definition of the χ^2 quantity being minimized.) This procedure is expected to diminish the influence of the disc on the fitted parameters. Masks of different opening angles were attempted: 30°, 60° and 100°. With increasing opening angle, the peak in the coefficient a_4 at $R \approx 12$ arcsec and the peak in the ellipticity curve at about the same radius diminished, as expected. Even for the largest mask, however, they had still not quite disappeared. This suggests that the disc also contributes significantly to the appearance of the isophotes near the minor axis, which in turn implies that the disc cannot be close to edge-on.

Alternatively, we tried to mask the whole galaxy except for a butterfly-shaped region centred on the major axis. We considered an opening angle of 30°. The best-fitting ellipses had constant ellipticity $\varepsilon \approx 0.4$. Since, for any given inclination, any contribution from the bulge will make the apparent

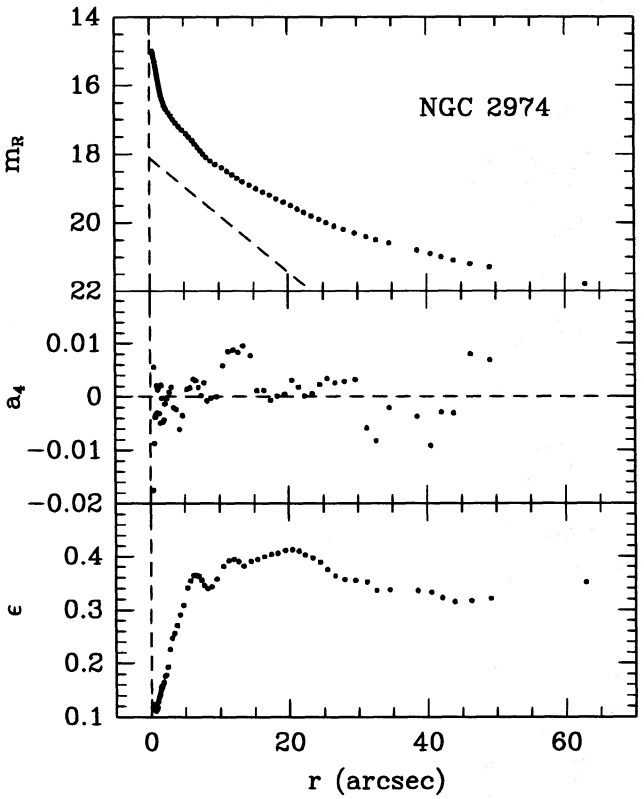

Figure 4. Shown are the observed R-band surface brightness, a_4 coefficient and ellipticity of NGC 2974, as a function of distance along the major axis. The dashed curve in the top panel is the exponential surface-brightness profile of the disc component of our standard model (which has $i = 57\overset{\circ}{.}5$, $R_d = 6$ arcsec and $m_d = 18.1$ mag arcsec^{-2}, cf. Section 5.1.2).

shape rounder, a lower limit to the inclination may be set by assuming that all the light in this region comes from the disc. We find in this way that $i \gtrsim 53°$. This is somewhat more stringent than the lower limit directly implied by the observed axial ratio of the isophotes, q_a: $i \geq \arccos q_a \gtrsim 47°$.

To make progress, additional assumptions must be made about the structure of the system. We assume the galaxy to consist of a bulge and a disc that is exponential in projection, motivated by the results in Fig. 3. As a first approach, we subtracted from the observed photometry exponential discs with different inclination angle i, central observed surface brightness m_d, and scalelength R_d. The resulting images were analysed, and it was determined which combinations of disc parameters led to 'reasonable' bulges (i.e., with smooth bulge surface-brightness profiles, and small a_4 at $R \approx 12$ arcsec). The best results were obtained for $55° \lesssim i \lesssim 65°$, $17 \lesssim m_d \lesssim 19$ mag arcsec^{-2} and $4 \lesssim R_d \lesssim 10$ arcsec. Faint discs (large values of m_d) only lead to reasonable bulges if combined with large values of R_d, and vice versa.

Both the maximum of a_4 (Fig. 4) and the minimum of the observed major axis dispersion (Fig. 1) occur at $R \approx 12$ arcsec. This radius thus very likely marks the position where the contribution of the disc light is largest. The values for f_{disc} in Fig. 3 suggest a smaller radius for this position, but this could be due to systematic errors in the double Gaussian decomposition, as discussed at the end of Section 2.4. Assuming that the maximum disc contribution is indeed at 12 arcsec, a rough estimate for the scalelength R_d of the disc can be obtained from arguments presented by Rix & White (1990). This yields $R_d \approx 8$ arcsec, somewhat larger than, but not inconsistent with, the results of Fig. 3. Comparing the amplitude of the a_4 coefficient with the deviations of the surface-brightness profile from an $R^{1/4}$ law with the results of the photometric models of Rix & White, we find $i \approx 59°$. This is consistent with estimates of the inclination as obtained from the analysis of neutral gas, ionized gas and dust in NGC 2974, as summarized in Section 1.

3.3 Seeing deconvolution

Seeing strongly influences the photometric quantities near the centre of a galaxy (e.g. Peletier et al. 1990). The light contribution of the disc in NGC 2974 is largest at $R \approx 12$ arcsec, however, far outside the region influenced by seeing. Consequently, the disc–bulge decompositions discussed in the previous section are not significantly influenced by seeing.

When calculating the predicted kinematics of NGC 2974 from the observed surface photometry, as will be done in Section 4, we will take the effects of seeing into account. However, we are not concerned with the question whether NGC 2974 has a central surface-brightness cusp and/or a central black hole, so a sophisticated image reconstruction scheme is not required for our purposes. We used a seeing-deconvolution scheme based on Lucy iteration. This yields, after only a few iterations, a deconvolved surface-brightness distribution that fits the observations within 0.05 mag after convolution with the point spread function (PSF). The deconvolved surface brightness is more centrally concentrated than the observed one, as would be expected.

The PSF was assumed to be a circular double Gaussian with the (observed) FWHM of 1.1 arcsec. In the absence of independent data to accurately determine the PSF *shape* for our observations, we chose the parameters of the double Gaussian as in van der Marel et al. (1994a). With these parameters, the PSF has broader wings than a single Gaussian. Its shape resembles that of one of Moffat's (1969) PSFs.

4 THE MODEL

4.1 Dynamical predictions

To model the observed kinematics of NGC 2974, we have extended the modelling technique pioneered by Binney, Davies & Illingworth (1990), and used later by van der Marel, Binney & Davies (1990) and van der Marel (1991). We first describe the dynamical model, and then discuss the underlying assumptions in Section 4.2.

We assume the galaxy to consist of a bulge and a disc. The disc surface brightness is assumed to be exponential with parameters R_d and m_d. The inclination i determines the axial ratio of the disc isophotes on the sky. For any fixed R_d, m_d and i, the surface brightness of the bulge is obtained by subtracting the disc surface brightness from the (seeing-deconvolved) observed surface brightness. One-component models can be constructed by choosing the disc to be infinitely faint.

4.1.1 *The dynamical model for the bulge*

The bulge surface brightness is deprojected under the assumption of axisymmetry using Lucy's algorithm to yield the three-dimensional luminosity density. The mass density ρ is then obtained upon assuming a constant mass-to-light ratio $(\mathscr{M}/L)_b$ for the bulge. Poisson's equation is solved using a multipole expansion to yield the potential of the bulge. Upon addition of the potential of the disc (Section 4.1.2), this yields the total potential Φ of the system. It is assumed that the distribution function of the bulge is of the form $f(E, L_z)$. The second radial velocity moment of the bulge stars, $\overline{v_R^2} \equiv \sigma_R^2$, and the second vertical velocity moment, $\overline{v_z^2} \equiv \sigma_z^2$, are then everywhere equal, while $\overline{v_R v_z} = 0$. The Jeans equations

$$\frac{\partial \rho \overline{v_z^2}}{\partial z} + \rho \frac{\partial \Phi}{\partial z} = 0, \tag{3a}$$

$$\frac{\partial \rho \overline{v_R^2}}{\partial R} + \rho \frac{\partial \Phi}{\partial R} + \frac{\rho}{R}[\overline{v_R^2} - \overline{v_\phi^2}] = 0, \tag{3b}$$

are solved for the unknowns $\overline{v_\phi^2}$ and $\sigma_R^2 = \sigma_z^2$. Part of the second azimuthal velocity moment $\overline{v_\phi^2}$ is then assigned to streaming, according to the prescription

$$\overline{v_\phi} = k\sqrt{\overline{v_\phi^2} - \sigma_R^2}\,. \tag{4}$$

This introduces a free parameter, k, which is the 'local equivalent' of the global rotational anisotropy parameter $(V/\sigma)^*$ of the bulge. The dynamical quantities are projected on to the sky (weighted with the mass density) to obtain predictions for the projected streaming and velocity dispersion of the bulge.

4.1.2 *The dynamical model for the disc*

The exponential disc is assumed to be infinitesimally thin, and to reside in the equatorial plane of the bulge. The surface mass density of the disc follows from its surface brightness upon assuming a constant mass-to-light ratio $(\mathscr{M}/L)_d$ for the disc. The disc potential is calculated from the surface mass density, as in Binney et al. (1990). Upon addition of the potential of the bulge (Section 4.1.1) this yields the total potential of the system. The Jeans equation for radial hydrostatic equilibrium is solved to predict the dynamics of the disc (given its mass density) in the total potential of the system.

The assumptions we make to solve the radial Jeans equation for the disc are similar to those used by Rix & White (1992) in their analysis of NGC 5322. The second radial velocity moment σ_R^2 in the disc is assumed to fall off as an exponential with a certain central value σ_{d0}^2 and exponential scalelength R_σ. The disc is also assumed to have $f = f(E, L_z)$. The vertical velocity dispersion σ_z^2 is thus equal to σ_R^2, and $\overline{v_R v_z} = 0$. The azimuthal velocity dispersion σ_ϕ^2 in the disc is assumed to be related to σ_R^2 according to the relation from epicyclic theory [equation (3-76) of Binney & Tremaine 1987],

$$\overline{(v_\phi - V_c)^2}/\sigma_R^2 = -B/(A - B), \tag{5}$$

where V_c is the circular velocity, and A and B are Oort's constants. The quantities V_c, A and B are all functions of radius. Equation (5) yields, for the azimuthal velocity dispersion σ_ϕ in the disc,

$$\sigma_\phi^2 = -(V_c - \overline{v_\phi})^2 + \frac{1}{2}\sigma_R^2\left(1 + \frac{R}{V_c}\frac{dV_c}{dR}\right). \tag{6}$$

The streaming velocity $\overline{v_\phi}$ in the disc (V_c minus the asymmetric drift) is now determined by the Jeans equation for radial equilibrium, which reduces to

$$\frac{\overline{v_\phi}}{V_c} = 1 - e^{-R/R_\sigma}\left(\frac{\sigma_{d0}^2}{2V_c^2}\right)\left(\frac{R}{R_d} + \frac{R}{R_\sigma} + \frac{1}{2}\frac{R}{V_c}\frac{dV_c}{dR} - \frac{1}{2}\right). \tag{7}$$

Taking into account the assumed inclination angle, one obtains predictions for the observed line-of-sight streaming and dispersion of the disc. No integration along the line of sight is required, since the disc is infinitesimally thin.

4.1.3 *The predicted velocity profiles*

Once the individual kinematics of the bulge and the disc have been calculated, it is assumed that both components have a Gaussian VP. The total VP predicted by the model is then a sum of two Gaussians, the normalizations of which are determined by the relative surface brightnesses of the two components.

4.2 Discussion of model assumptions

4.2.1 *Model assumptions for the bulge*

Our model assumes that the bulge: (i) is axisymmetric; (ii) has a constant mass-to-light ratio; and (iii) has $f = f(E, L_z)$.

Our assumption of axisymmetry implies that we discard the weak spiral structure seen on deep optical images (Buson et al. 1993). In addition, we discard any triaxiality of the bulge and non-circularity of the disc. In reality, the bulge of NGC 2974 is likely to be slightly triaxial. It has an observed isophote twist of $\sim 5°$ and small $\sin 4\theta$ deviations of the isophotes from ellipses (Buson et al. 1993). Amico et al. (1993) demonstrate that the velocity field of the ionized gas in NGC 2974 is best understood by assuming the gas to be on elliptic, rather than circular, orbits. Models indicate an axial ratio $b/a \approx 0.8$ for the mass distribution in the equatorial plane. The corresponding axial ratio of the potential in the equatorial plane is $b/a \gtrsim 0.9$, so our assumption of axisymmetry ($b/a \equiv 1$) is not expected to introduce large errors, also since no minor axis rotation is observed.

In a study of 37 galaxies, van der Marel (1991) found some evidence for a general increase of $\mathscr{M}/L$ with radius in elliptical galaxies. However, evidence for this came primarily from the data-points at large radii; a constant $\mathscr{M}/L$ model generally provides an adequate fit to the data inside ~ 1 effective radius. Our kinematic data for NGC 2974 do not extend beyond 15 arcsec, and our assumption of constant $\mathscr{M}/L$ thus seems justified. On the other hand, the best-fitting model of Amico et al. (1993) for the observed ionized gas kinematics in NGC 2974 does have a mild increase in $\mathscr{M}/L$ in the inner 15 arcsec.

Models with a distribution function of the form $f(E, L_z)$ have the advantage that the Jeans equations form a closed set (other assumptions to close the Jeans equations are also

possible: see, for example, Bacon 1985; van der Marel & Cinzano 1992). Binney et al. (1990) and van der Marel (1991) found that $f(E, L_z)$ models generally predict too much motion on the major axis, indicating that real galaxies have more radial motion than do models with $f(E, L_z)$. The differences between the model predictions and the data, however, are generally small. For NGC 2974, a galaxy observed to have an unusually large amount of motion on the major axis, the assumption of $f(E, L_z)$ might well be close to the truth. The use of equation (4) to calculate the streaming of the bulge is somewhat arbitrary, but none of our results depends heavily on this.

4.2.2 *Model assumptions for the disc*

Our model for the disc is much less realistic than that for the bulge. Our simplifying assumptions for the disc dynamics are motivated by the fact that the shape of the velocity dispersion ellipsoid is only extremely poorly constrained by the data anyway. Hence there is little justification in making a very detailed model. Our main aim was to capture the essential physics of the disc, in order to obtain a realistic estimate of the asymmetric drift without invoking too many free parameters and functions that could not plausibly be determined from the data anyway. The shape of the velocity dispersion ellipsoid is unknown, even for isolated disc galaxies, so we have no hope of being able to determine it for NGC 2974, where even the presence of the disc is not obvious.

Our model assumes that the exponential disc: (i) is infinitesimally thin; (ii) has a constant mass-to-light ratio; (iii) has an exponentially falling σ_R^2 profile; (iv) has $\sigma_z^2 = \sigma_R^2$; and (v) has σ_ϕ^2 satisfying the epicyclic theory relation. We neglect the vertical structure of the disc, because it is not well constrained by the data. The assumption of constant mass-to-light ratio was discussed in Section 4.2.1. Assumptions (iii) and (iv) receive some justification from the fact that σ_R^2 in our own Galaxy and σ_z^2 in face-on spirals are observed to fall exponentially with galactocentric distance (Lewis & Freeman 1989; van der Kruit & Freeman 1986). In our own Galaxy $\sigma_z^2/\sigma_R^2 \approx 0.5$. The choice $\sigma_z^2/\sigma_R^2 = 1$ for NGC 2974 is one of convenience. It is not consistent with the assumed vertical extent of the disc. On the other hand, the choice $\sigma_z^2 = 0$ that *is* consistent with the assumed vertical extent of the disc does not seem very realistic either. In fact, we constructed both models with $\sigma_z^2/\sigma_R^2 = 1$ and models with $\sigma_z^2 = 0$, but found the results to be very similar (apart, obviously, from the normalization of σ_R^2 in the disc). None of our main conclusions depends sensitively on the assumed ratio σ_z/σ_R. Assumption (v) is not expected to be very realistic either, but at least it provides a well defined relation between σ_ϕ and σ_R. The relation dictated by epicyclic theory only strictly holds for discs that are much colder than the one in NGC 2974 (which has $V/\sigma \gtrsim 3$, cf. Fig. 3). In fact, the epicyclic theory relation can introduce severe systematic errors even for the disc of our own Galaxy (Kuijken & Tremaine 1992; Evans & Collett 1993; Cuddeford & Binney 1994).

4.2.3 *Model assumptions for the velocity profile*

It is assumed that both the bulge and the disc have a Gaussian VP. This assumption is motivated by the belief that the overall shape of the observed VP will be determined mainly by differences in the kinematic properties of the two components, rather than by the shape of their individual VPs.

None the less, let us stress that there is no reason why the VPs of the individual components should indeed be Gaussian. In fact, observations seem to indicate that observed VPs are significantly asymmetric whenever there is rotation (vdMF; van der Marel et al. 1994a). This is not always necessarily the result of the presence of a kinematically distinct subcomponent, because asymmetric VPs also arise naturally in one-component models of galaxies (Dehnen & Gerhard 1993; vdMF; Evans 1993, 1994; van der Marel et al. 1994b). As will be demonstrated in Section 5, however, the argument for claiming the presence of an embedded stellar disc in NGC 2974 is not based primarily on the observed asymmetry of the VPs, but rather on the large amount of rms motion on the major axis.

4.3 The comparison of model predictions with data

Once the predicted VPs on the sky are calculated for a given set of model parameters, they are convolved with the seeing PSF and sampled over the pixel size and the width of the slit, so as to mimic the observational set-up of our spectroscopic observations. This yields one predicted VP for each galaxy spectrum that was analysed. The shape of the PSF for the spectroscopic observations was assumed to be a circular double Gaussian, as in Section 3.3. No independent determination of the seeing FWHM for the spectroscopic data was available. It was therefore estimated by convolving the seeing-deconvolved surface photometry (described in Section 3.3) with PSFs of different FWHM. The PSF that resulted in the best fit to the observed intensity profile along the slit, as observed spectroscopically, had FWHM ≈ 1.9 arcsec. Even though the procedures we adopt for seeing-deconvolving our photometry and seeing-convolving our dynamical predictions are not perfect, they do capture the essence of the spatial smearing of the data. This is especially important for the modelling of the observed kinematics close to the centre.

In comparing the model predictions with the data it is necessary to mimic as closely as possible the observational situation. For example, it is better *not* to compare the true mean and dispersion of the model VP with the parameters V and σ obtained by fitting a Gaussian VP to the data. This can easily introduce systematic errors of order 20 per cent (vdMF). In practice, we therefore first calculate the Fourier transform of a predicted VP, and then do a χ^2 fit over a restricted range of wavenumbers in Fourier space to determine the predicted VP parameters (V, σ, h_3, h_4), defined as in Section 2.2. These can then be compared with the observed values. The same lower and upper wavenumber cut-offs are used as in analysing the data. We have not attempted to model the fact that the Fourier Fitting Method gives unequal weight to different frequency components, due to the fact that not all frequency components are present in the template spectrum in equal amounts (which is in part due to the instrumental resolution). The correct modelling of the low wavenumber cut-off was found to be important. The higher the low wavenumber cut-off, the more biased the Fourier Fitting Method becomes to the low-dispersion kinematic component. The modelling of the upper wavenumber cut-off was generally found to be unimportant.

5 RESULTS AND DISCUSSION

5.1 Stellar kinematics and velocity profiles

5.1.1 *One-component models*

First we tried to fit the observed stellar kinematics without invoking the presence of an embedded stellar disc. The main difficulty in such a model is to fit the ratio v of the projected rms velocity $\sqrt{V^2+\sigma^2}$ on the major and the minor axes. The value of v predicted by a one-component $f(E, L_z)$ model increases with decreasing inclination (for example, van der Marel 1991). To fit the observed profile of v as a function of projected galactocentric distance on the sky we had to choose the inclination as small as $i \approx 48°$. By setting the parameter k (equation 4) equal to 1.06 and $(\mathscr{M}/L)_R = 3.3\, h_{50}$ (in solar units), we in fact obtained an excellent fit to the observed V and σ along all three available slit positions. However, the assumed inclination implies that the intrinsic axial ratio of the model is $q_t \lesssim 0.25$ throughout. This is unrealistically flat. Elliptical galaxies with apparent flattening $\lesssim 0.3$ are never observed (Binney & de Vaucouleurs 1981). We thus conclude that NGC 2974 most likely has a stellar disc. Without such a disc it is not possible to fit the large amount of rms motion on the major axis, whilst also maintaining a realistic flattening for the galaxy. In addition, it remains to be seen whether a model without a stellar disc would be able to explain satisfactorily the pointedness of the isophotes and the asymmetry of the major axis VPs.

5.1.2 *Disc–bulge models*

By introducing a disc in the model, the number of free parameters increases to such an extent that a full exploration of the parameter space becomes unfeasible. To reduce the number of free parameters, we therefore only considered models in which the bulge is an oblate isotropic rotator ($k = 1$) and in which the bulge and the disc have the same $(\mathscr{M}/L)$. The $(\mathscr{M}/L)$ determines the velocity normalization, and was, for each combination of disc parameters, chosen so as to optimize the fit to the minor axis dispersion measurements.

We started by considering models for the disc with $R_d = 6$ arcsec, as indicated by Fig. 3, and $i = 57.^\circ5$, which is a typical value obtained from observations and models of neutral and ionized gas in NGC 2974 (cf. Section 1). This leaves as free parameters the central (R-band) disc surface brightness m_d and the parameters σ_{d0} and R_σ that determine the radial velocity dispersion in the disc. The best fit (as judged by eye) to the observed (V, σ, h_3, h_4) for the three available slit position angles was obtained for $m_d = 18.1$ mag arcsec^{-2}, $R_\sigma = 4.3$ arcsec and $\sigma_{d0} = 205$ km s^{-1}. We will refer to the model with these parameters as the 'standard model'. Figs 5(a)–(c) show the data-points and the predictions of the model with these parameters (solid curves). Nearly all features seen in the data are adequately fitted. The mass-to-light ratio of the model is $(\mathscr{M}/L)_R = (2.9 \pm 0.3)\, h_{50}$, somewhat higher than what should be expected for a galaxy of this luminosity (van der Marel 1991). The error bar is the formal error of the fit to the minor axis σ-measurements, and does not take any of the uncertainties in the model into account. The total (R-band) magnitude of the disc is $R_{Td} = 12.89$, implying a ratio of total disc luminosity to total bulge luminosity of 0.07. Fig. 6 shows, as a function of galactocentric distance, the fraction of the light observed on the major axis that is due to the disc. The maximum contribution of the disc is ~25 per cent, at $R \approx 9$ arcsec. Also shown are the (projected) mean velocity V and velocity dispersion σ of the bulge and the disc.

The observations of neutral gas, ionized gas and dust (Section 1), the double Gaussian decomposition of the observed VPs (Section 2.4), and the disc–bulge decomposition of the photometry (Section 3) all indicate that the inclination angle i, the central R-band disc surface brightness m_d and the disc scalelength R_d must be sought in the range $55° \lesssim i \lesssim 65°$, $17 \lesssim m_d \lesssim 19$ mag arcsec^{-2} and $4 \lesssim R_d \lesssim 10$ arcsec. Any other combination of disc parameters would violate at least one of the observations discussed before. We therefore sought other acceptable models with parameters in these ranges. We found that the fit of the model to the kinematics and the VPs remained acceptable only if the inclination of the disc, its scale radius and its central observed magnitude were all simultaneously decreased or simultaneously increased with respect to the standard model. Apparently, both small, bright discs and large, faint, more highly inclined discs can fit the data. The total luminosity of the disc is therefore better constrained than either m_d, R_d or i. As an example, the dashed curves in Fig. 5 show the predictions of a model with $i = 62.^\circ5$, $m_d = 18.5$ mag arcsec^{-2} and $R_d = 8$ arcsec. The fit of this model to the data is also acceptable. The total (R-band) magnitude of the disc in this model is $R_{Td} = 12.83$, and the ratio of total disc luminosity to total bulge luminosity is 0.08.

By considering models with $k = 1$ and $(\mathscr{M}/L)_d = (\mathscr{M}/L)_b$, we obtain good fits to the observed kinematics and VPs. There is thus no compelling evidence to cause us to assume that either $k \neq 1$, or $(\mathscr{M}/L)_d \neq (\mathscr{M}/L)_b$. On the other hand, we did not make a detailed study of models with $k \neq 1$ or with $(\mathscr{M}/L)_d \neq (\mathscr{M}/L)_b$, so cannot exclude them either. If the disc consists of young massive stars, it might have a smaller $(\mathscr{M}/L)$ than the bulge. In principle, one could hope to constrain the ratio between $(\mathscr{M}/L)_d$ and $(\mathscr{M}/L)_b$ from a comparison of photometry in different bands, but this is complicated by the presence of dust in NGC 2974.

We intentionally did not plot in Fig. 6 the results of the double Gaussian decomposition of the major axis VPs shown previously in Fig. 3. The latter quantities were obtained from data that had been low-wavenumber filtered, and should thus not be compared directly with true physical characteristics of the model. To illustrate this, note that our models take the low-frequency filtering of the data into account and adequately fit the observed h_3 and h_4. None the less, the fraction of the light contributed by the disc in our models is only half of that indicated by Fig. 3. This demonstrates that, by filtering low Fourier wavenumbers, one tends to overestimate the importance of the disc component. Fig. 7 illustrates this in a different way. Plotted are the predicted major axis quantities V and σ for the standard model (solid curves; the same as in Fig. 5), as well as the true mean streaming and dispersion of the model (dashed curves), not taking the seeing and low-wavenumber Fourier filtering into account. With the proper modelling of the observational set-up (solid curves), the amplitude of the predicted rotation curve is significantly higher, mainly due to the fact that the

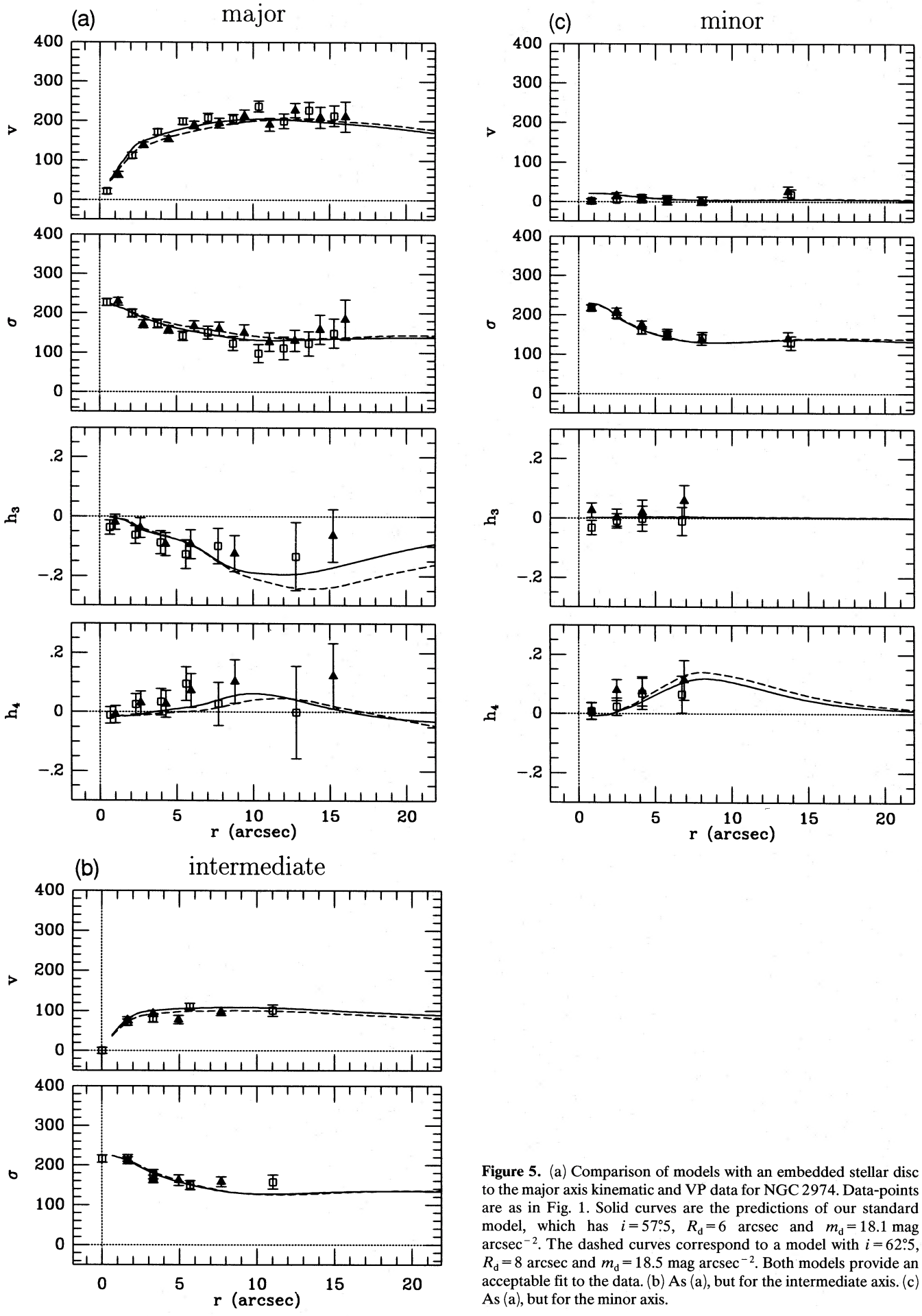

Figure 5. (a) Comparison of models with an embedded stellar disc to the major axis kinematic and VP data for NGC 2974. Data-points are as in Fig. 1. Solid curves are the predictions of our standard model, which has $i = 57.^{\circ}5$, $R_d = 6$ arcsec and $m_d = 18.1$ mag arcsec^{-2}. The dashed curves correspond to a model with $i = 62.^{\circ}5$, $R_d = 8$ arcsec and $m_d = 18.5$ mag arcsec^{-2}. Both models provide an acceptable fit to the data. (b) As (a), but for the intermediate axis. (c) As (a), but for the minor axis.

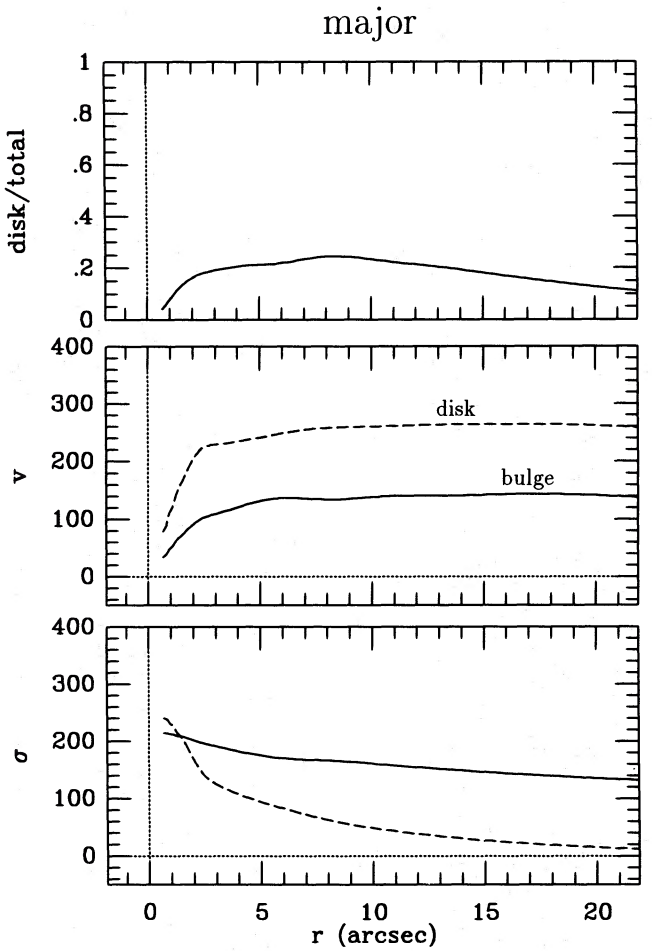

Figure 6. The top panel shows, for our standard model, the fraction of the light contributed by the disc component along the major axis, after seeing convolution. The middle panel shows the major axis mean velocities of the bulge (solid curve) and disc (dashed curve). The bottom panel shows the respective velocity dispersions.

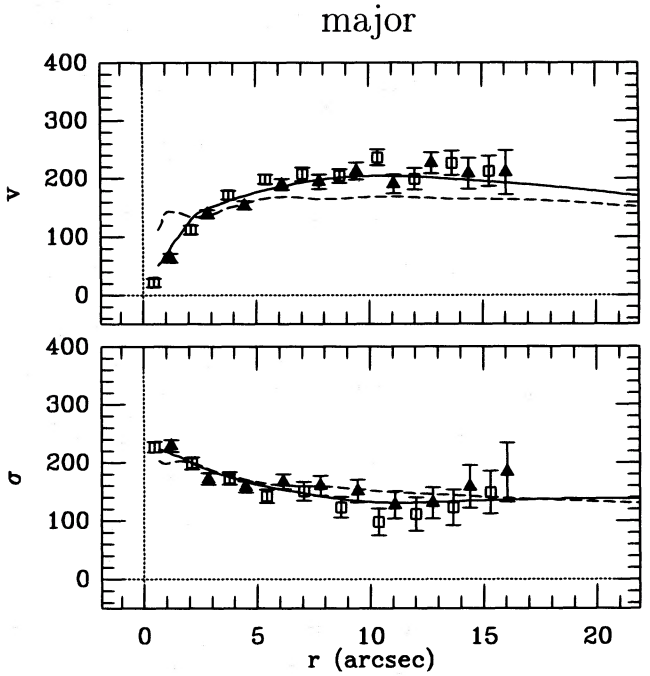

Figure 7. Major axis V and σ for NGC 2974. The solid curves are the predictions of our standard model as in Fig. 5. The dashed curves show for comparison the predictions for the true rotation and dispersion of the model, when the modelling of the low-wavenumber filtering and the seeing convolution of the kinematics are omitted. The differences between the curves illustrate the importance of paying attention to details in the dynamical modelling.

low-wavenumber Fourier filtering increases the relative importance of the disc.

Our model parameters agree well with the preliminary results discussed by Cinzano & van der Marel (1993). There are some differences in the details though, because in our previous work we neglected the effects of seeing and low-wavenumber Fourier filtering. However, the disc-to-bulge ratio reported here is very much the same as the one we reported previously. Our results are also, on the whole, consistent with those of Scorza (1993b), who did photometric and kinematic disc–bulge compositions for a sample of elliptical galaxies, including NGC 2974. She finds $i \approx 58°.5$, and a ratio of total disc luminosity to total bulge luminosity of 0.10 ± 0.05. The main difference in our results is in the rotation of the bulge component. She finds ~ 180 km s^{-1} for the maximum rotation of the bulge, whereas we find ~ 140 km s^{-1} (cf. Fig. 6). Scorza reports $(V/\sigma)^* = 1.6$ for the bulge component, whereas our standard model has k, and thus $(V/\sigma)^*$, equal to 1. For her sample of elliptical galaxies with discs, Scorza finds a correlation between the surface brightnesses of the bulge components and their $(V/\sigma)^*$. NGC 2974 was found not to fit the correlation because of the remarkably high $(V/\sigma)^*$. However, when $(V/\sigma)^* = 1$ is used, as found here, it fits the correlation well.

5.1.3 *Stability and substructure of the stellar disc*

Buson et al. (1993) photometrically studied the presence of substructure in NGC 2974, essentially by subtracting a smooth galaxy model from the observed image. They report the presence of a weak two-armed spiral structure, extending out to $R \approx 16$ arcsec. We calculated the dynamical 'temperature' of the stellar disc in our models, as quantified by the Toomre Q parameter (Toomre 1964),

$$Q \equiv \frac{\sigma_R \kappa}{3.36\, G\Sigma}, \tag{8}$$

where Σ is the surface mass density of the disc and κ is the epicycle frequency,

$$\kappa \equiv \frac{3}{R}\frac{\partial \Phi}{\partial R} + \frac{\partial^2 \Phi}{\partial R^2}. \tag{9}$$

Fig. 8 shows the results for our standard model (solid curve) and for the alternative model in Fig. 5 (dashed curve).

Our dynamical model for the disc in NGC 2974 involves many assumptions. The dispersion σ_R, and hence Q, is therefore not very well determined. First, the line-of-sight velocity dispersion we derive for the disc might be in error if the true VP of either the disc or the bulge were to be significantly

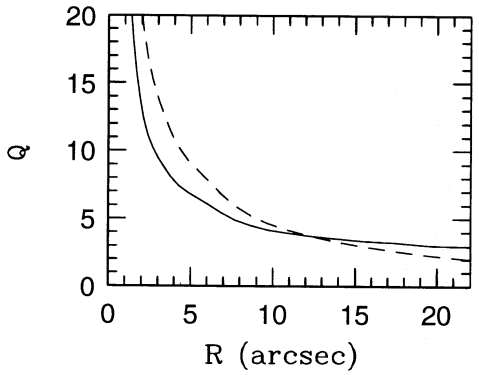

Figure 8. Toomre's Q parameter of the stellar disc, for our standard model (solid curve) and for the alternative model of Fig. 5 (dashed curve). We do not plot Q for the outer parts of the disc, because the parameters of the disc were determined from kinematic data with $R \lesssim 16$ arcsec.

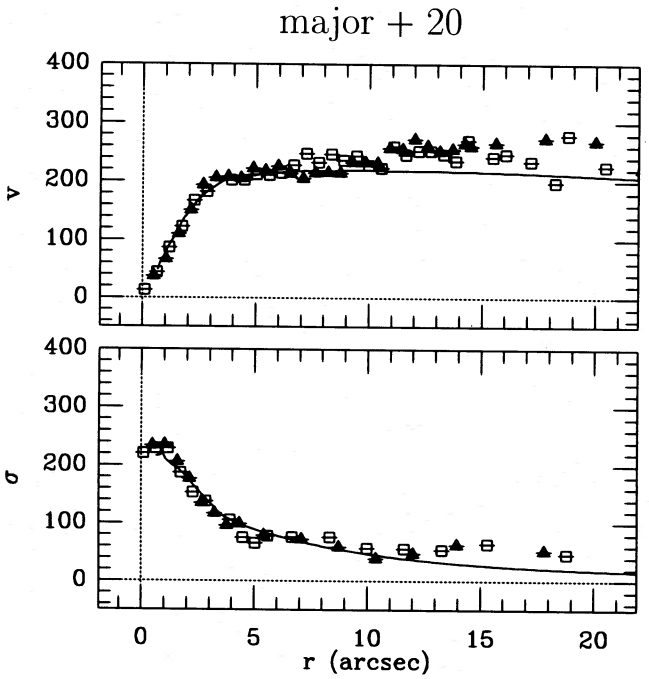

Figure 9. The data-points are the mean velocity (top panel) and velocity dispersion (bottom panel) of the ionized gas in NGC 2974, along an axis with position angle 20° from the major axis (from Amico et al. 1993 and Zeilinger et al., in preparation). Formal error bars on the data-points are not available, but can be estimated from the scatter between neighbouring points. The curves are the predictions of our model for the gas disc, as described in the text.

non-Gaussian (see Section 4.2.3). Secondly, the line-of-sight dispersion of the disc is a weighted mixture of the principal velocity dispersion components. The inferred value of σ_R thus depends on the assumed ratio σ_z/σ_R. This ratio is poorly constrained by the data and we rather arbitrarily choose it to be unity in the model (see Section 4.2.2). Thirdly, at ~ 10 arcsec, σ_R becomes comparable to the instrumental resolution of our data. So for $R \gtrsim 10$ arcsec, we cannot exclude the possibility that the σ_R of our models is an overestimate. The results in Fig. 8 should thus be taken as a very rough estimate only.

The shape of the $Q(R)$ profiles in Fig. 8 is similar to that of the disc of our own Galaxy, which also has a sharp increase at small radii (Lewis & Freeman 1989). The Q values for NGC 2974 are much larger though. The fact that $Q > 1$ implies that the disc is locally stable to axisymmetric perturbations (Binney & Tremaine 1987). The fact that Q appears to be much larger than 1 makes the presence of a two-armed spiral structure somewhat puzzling. The mechanism of swing amplification is inefficient for $Q \gtrsim 3$, and, in addition, the stability of the disc in NGC 2974 is increased by the fact that it is embedded in the potential of a prominent bulge component (which does not respond to perturbations in the disc). On the other hand, the amplitude of the observed spiral structure in NGC 2974 is not strong, so swing amplification might still have played a role. An alternative explanation for the observed spiral structure would be that at some distant time gas collapsed locally, formed stars and sheared out. This would be expected to lead to many little spiral arms, however, rather than to the observed two-armed feature.

5.2 Ionized gas kinematics

Fig. 9 displays the observed V and σ for the ionized gas in NGC 2974, along a slit that makes an angle of 20° with the major axis. These data were obtained in the context of the ESO Key Project 'A search for dark matter in elliptical galaxies', and were presented by Amico et al. (1993). The observational set-up and data analysis will be described in detail by Zeilinger et al. (in preparation). The kinematic quantities were derived by fitting a Gaussian to the [N II]6583-Å emission line at each radius. The slit width of the observations was 1.5 arcsec and the pixel size along the slit was 0.55 arcsec. We determined the effective seeing of the observations (i.e., the spatial smearing due to the combined effects of seeing and guiding errors) from the observed continuum intensity profile along the slit (as for our spectroscopic observations of the stellar kinematics, cf. Section 4.3), yielding a FWHM of 2.8 arcsec.

We model the ionized gas kinematics of NGC 2974 by assuming the gas to be in individual clumps that orbit as test particles in the potential defined by the bulge and the embedded stellar disc. The total mass of the ionized gas itself is small, so it does not contribute significantly to the total potential of the system. We assume the gas disc to be infinitesimally thin and exponential. Our model for the kinematics of the gas disc is similar to that of the stellar disc: we assume the radial velocity dispersion of the gas disc to fall off exponentially as a function of radius with central value $\sigma_{\mathrm{d0,gas}}$ and radial scalelength $R_{\sigma,\mathrm{gas}}$. The kinematics of the gas are then determined by the Jeans equation for radial hydrostatic equilibrium, as for the case of the stellar disc discussed in Section 4.1.2. We take the seeing and observational set-up into account as described above.

The curves in Fig. 9 show the predictions of our model, taking $\sigma_{\mathrm{d0,gas}} = 170$ km s^{-1}, $R_{\sigma,\mathrm{gas}} = 4.3$ arcsec, and taking the parameters of the bulge and the stellar disc as in our standard model of Section 5.1. The scale radius of σ_R in the gas disc is the same as in the stellar disc, but the central value of σ_R is somewhat smaller than in the stellar disc. The mass density of the gas disc cannot easily be determined from

observations. The Hα surface brightness (Buson et al. 1993) is critically sensitive to the unknown ionization fraction of the gas. In the absence of other constraints, we therefore assumed the exponential scale radius of the gas disc to be the same as for the stellar disc (6 arcsec). The model in Fig. 9 provides an excellent fit to both the observed streaming velocities and the observed velocity dispersions. This indicates that the observed streaming velocities of the ionized gas are consistent with the potential and circular velocity derived from the stellar kinematics, and the asymmetric drift implied by the observed non-zero velocity dispersion of the gas.

We also constructed an alternative model for the ionized gas disc in which the velocity dispersion σ_R of the gas is 75 km s^{-1} throughout. In this model, the predicted velocity dispersion has a central peak due solely to the seeing convolution of the rotation curve near the centre. The central velocity dispersion of the gas predicted by this model is ~ 30 km s^{-1} smaller than the observed value. On the other hand, the velocity dispersions estimated from the data might contain significant systematic errors. They were obtained by fitting Gaussians to the [N II] emission lines, which might have been significantly non-Gaussian as a result of the seeing convolution. So even though our model in Fig. 9 has an increasing velocity dispersion towards the centre, we cannot rule out models in which the velocity dispersion in the gas disc is constant. A detailed study of the observed emission-line profiles, or data of higher spatial resolution are required to settle this issue.

In Fig. 10, we show the mean velocities and velocity dispersions of the *stellar* disc in our standard model for NGC 2974, similar to Fig. 6, but convolved with the seeing and observational set-up of the ionized gas observations. The data-points show the observed ionized gas kinematics, as in Fig. 9. Clearly, the kinematics of the ionized gas disc are strikingly similar to the kinematics of the stellar disc. This suggests a common evolutionary history for these components. One possibility could be that the ionized gas was in fact produced by stars in the stellar disc, in particular by planetary nebulae, a scenario discussed by Fillmore, Boroson & Dressler (1986).

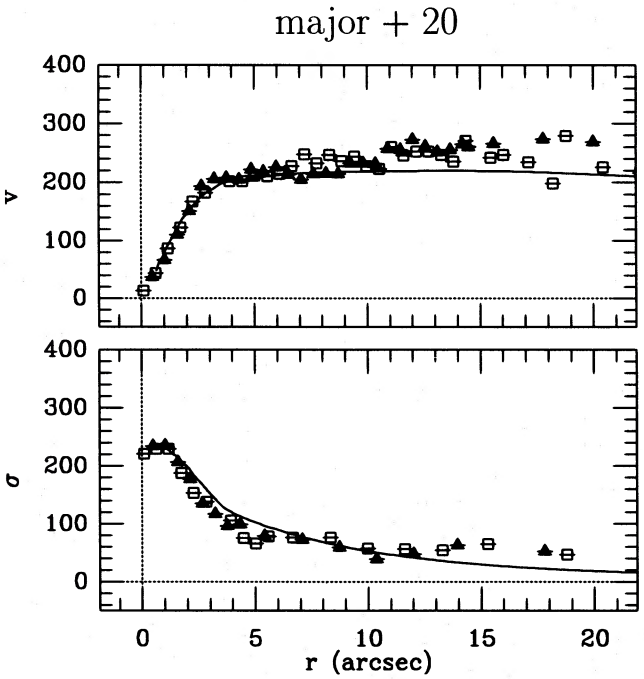

Figure 10. The data-points are the mean velocity and velocity dispersion of the ionized gas, as in Fig. 9. The curves are the mean velocity and velocity dispersion of the *stellar* disc in our standard model, convolved with the seeing and observational set-up of the ionized gas observations. Note the similarity between the kinematics of the stellar disc and the ionized gas disc in NGC 2974.

Amico et al. (1993) modelled the observed ionized gas kinematics in NGC 2974 using a triaxial model with varying mass-to-light ratio and gas moving on elliptic closed orbits in the equatorial plane. By fitting to the observed streaming velocities along four different position angles, the triaxial shape of the galaxy and the run of the mass-to-light ratio as a function of radius could be determined. The mass-to-light ratio in the best-fitting model increases slowly with radius. At 15 arcsec the value is $(\mathscr{M}/L)_B \approx 3.5\, h_{50}$, corresponding to $(\mathscr{M}/L)_R \approx 1.9\, h_{50}$. This is significantly smaller than the value we deduce from the stellar kinematics, $(\mathscr{M}/L)_R \approx (2.9 \pm 0.3)\, h_{50}$. The discrepancy might be the result of a number of differences between our modelling approach and that of Amico et al. Most likely, it is due to their use of simple closed orbits. This neglects the asymmetric drift implied by the bulk (non-thermal) velocity dispersion of the ionized gas. As a result, the mass-to-light ratio of the gravitating matter will tend to be underestimated. It has been reported before, by Caldwell (1984) and Caldwell, Kirshner & Richstone (1986) for elliptical galaxies, and by Fillmore et al. (1986) and Kent (1988) for spiral bulges, that the streaming velocity of the ionized gas in galaxies is often smaller than the circular velocity as determined from the stellar kinematics. Sometimes this can be explained by constructing triaxial models (Bertola et al. 1991). However, for NGC 2974, the $\mathscr{M}/L$ derived from the ionized gas kinematics (under the assumption of closed orbits) is smaller than that derived from the stellar kinematics, even when a triaxial model is used (Amico et al. 1993).

5.3 H I kinematics – the dark halo

Kim et al. (1988) studied the H I disc in NGC 2974, which extends out to 120 arcsec from the centre ($\sim 3.6\, R_e$). The observed rotational velocity at the edge of the disc is ~ 291 km s^{-1}. This velocity can be compared to the circular velocity of our (constant $\mathscr{M}/L$) models. The total mass implied by the observed luminosity of NGC 2974 and the mass-to-light ratio of our standard model is $M_{\rm lum} = 2.4 \times 10^{11}\ h_{50}^{-1}$ $M_\odot$. As a result, the circular velocity of our model falls off in the outer parts as $V_c = (410\ \text{km s}^{-1})\ (R/R_e)^{-1/2}$. For an assumed inclination of $i = 57\overset{\circ}{.}5$ the observed streaming velocity for a disc of test particles on circular orbits in the equatorial plane is thus expected to fall off as $V_c = (346\ \text{km s}^{-1})(R/R_e)^{-1/2}$. At 120 arcsec, the predicted velocity is 183 km s^{-1}, much smaller than the observed H I velocity. This implies that NGC 2974 must have a dark halo with $M_{\rm halo}(< 3.6\, R_e) = 3.6 \times 10^{11}\ h_{50}^{-1}\ M_\odot$.

Bertola et al. (1993) recently studied the properties of the dark haloes of a small sample of elliptical galaxies, including NGC 2974. In analogy with the case for spiral galaxies, they suggest that the mass density of the dark haloes is well fitted with a formula of the form $\rho(r) \propto (a^2 + r^2)^{-1}$, with $a \approx 1.2\, R_e$.

The derived value for $M_{\rm halo}(<3.6\,R_{\rm e})$ then implies that $M_{\rm halo}(<0.5R_{\rm e})=5\times10^{9}\ \ h_{50}^{-1}\ {\rm M}_{\odot}$. The corresponding circular velocity is $V_{\rm c,halo}(0.5\,R_{\rm e})=79$ km s^{-1}. This is much smaller than the circular velocity of the luminous matter at this radius, which is the radius of our last kinematic datapoint (cf. Section 2). Since $V_{\rm c}^2=V_{\rm c,lum}^2+V_{\rm c,halo}^2$, the presence of a dark halo does not alter any of the conclusions that we have drawn by applying our constant $\mathscr{M}/L$ models to kinematic data inside $0.5\,R_{\rm e}$.

6 CONCLUSIONS

We present new spectroscopic data for the E4 galaxy NGC 2974, along the major, the minor and an intermediate axis. From the data we determine rotational velocities, velocity dispersions and deviations of the VPs from a Gaussian. On the major axis, NGC 2974 rotates rapidly ($V/\sigma\approx1$). The VPs are asymmetric, with the asymmetry changing sign upon going from one side of the nucleus to the other. The asymmetry is such that there is an excess of stars at low velocities. The kinematic and VP data, the observed pointedness of the isophotes, and previous detections of discs of neutral gas, ionized gas and dust in NGC 2974, strongly suggest the presence of an embedded stellar disc.

We make detailed dynamical models for NGC 2974, with an infinitesimally thin exponential stellar disc embedded in the equatorial plane of an axisymmetric bulge component. The Jeans equations are solved to predict the dynamics of the two components. The results are projected on to the sky, integrated along the line of sight, and compared with the observed kinematics and VPs. The main advantage of our technique is that only disc–bulge combinations that are in hydrostatic equilibrium in the total potential of the system are considered. This significantly reduces the freedom in the interpretation of the data. We explicitly model the filtering of low Fourier frequencies applied to the data, and show that this is important.

To fit the observed ratio of major to minor axis rms motion without invoking the presence of a stellar disc requires the galaxy to have an intrinsic axial ratio $q_{\rm t}\lesssim0.25$. This is unrealistically flat: elliptical galaxies with apparent flattening $q_{\rm a}\lesssim0.3$ are never observed. In addition, it remains to be seen whether a model without a stellar disc would be able to explain satisfactorily the pointedness of the isophotes and the asymmetry of the major axis VPs.

When an embedded stellar disc is included in the model, an acceptable fit can be obtained to all the available photometric and kinematic data, including the observed deviations of the VPs from a Gaussian. Our 'standard' model has inclination $i=57\overset{\circ}{.}5$ consistent with estimates obtained from the observations of neutral and ionized gas in NGC 2974, exponential disc scalelength $R_{\rm d}=6$ arcsec (i.e., $1.12\,h_{50}^{-1}$ kpc) and central *face-on* R-band surface brightness $m_{\rm d,90}=18.8$ mag arcsec^{-2}. This corresponds to $m_{\rm d,90}=20.6$ in B, within the observed range for spirals (Freeman 1970; Boroson 1981; Disney & Phillips 1985). The disc contributes ~7 per cent of the total light. The maximum contribution of the disc is ~25 per cent, at $R\approx9$ arcsec. The disc has $(V/\sigma)\gtrsim3$, indicating that the disc is primarily rotationally supported. The fit to the kinematics and the VPs remains acceptable if the inclination of the disc, its scale radius and its central observed magnitude are all simultaneously decreased or increased with respect to the standard model. Apparently, both small, bright discs and large, faint, more highly inclined discs can fit the data. The total luminosity of the disc is better constrained than any one of $m_{\rm d}$, $R_{\rm d}$ or i.

Ionized gas kinematics for NGC 2974 were presented by Amico et al. (1993) and Zeilinger et al. (in preparation). We modelled these data by assuming the gas to consist of individual clumps that orbit as test particles in the potential defined by the bulge and the embedded stellar disc. The run of the velocity dispersion in the gas disc is chosen to fit the observed velocity dispersions. The streaming velocities of the ionized gas are then predicted using the equation of radial hydrostatic equilibrium. The model provides an excellent fit to the observed streaming velocities, indicating that these are consistent with the potential derived from the stellar kinematics, and the asymmetric drift implied by the observed non-zero velocity dispersion of the gas. The kinematics of the ionized gas disc in NGC 2974 are strikingly similar to the kinematics of the stellar disc, suggesting a common evolutionary history for these components.

The total luminous mass of NGC 2974 is $M_{\rm lum}=2.4\times10^{11}\ h_{50}^{-1}\ {\rm M}_{\odot}$. The H I data presented by Kim et al. (1988) indicate that NGC 2974 has a dark halo with $M_{\rm halo}(<3.6R_{\rm e})=3.6\times10^{11}\ h_{50}^{-1}\ {\rm M}_{\odot}$. In the region of our spectroscopic data ($\lesssim0.5\,R_{\rm e}$), the dynamical influence of the dark halo is negligible.

Our study of NGC 2974 demonstrates that it most likely has an embedded stellar disc. At a higher inclination angle, NGC 2974 would presumably have been classified as an S0, rather than as an elliptical galaxy. Given the observational evidence for weak spiral structure, it is not even excluded that NGC 2974 is in fact an Sa galaxy with an unusually low disc-to-bulge ratio. Many more galaxies like NGC 2974 might exist. If the discs in these galaxies are either less luminous or less inclined than in NGC 2974, they will be very hard to detect.

ACKNOWLEDGMENTS

The results presented in this paper are based on observations done at the European Southern Observatory, La Silla, Chile. We are indebted to John Danziger for taking the spectra analysed in Section 2 and the direct image analysed in Section 3, to Werner Zeilinger for doing the basic reduction of the spectra, to Lucio Buson for providing us with his reduced version of the direct image of NGC 2974, to Tim de Zeeuw and Francesco Bertola for support throughout this project, to James Binney for developing the technique to solve the Jeans equations for $f(E, L_z)$ models and for providing useful comments that helped improve the presentation of the paper and to Cecilia Scorza and Hans-Walter Rix for useful discussions.

REFERENCES

Amico P. et al., 1993, in Danziger I. J., Zeilinger W. W., Kjär K., eds, Structure, Dynamics and Chemical Evolution of Elliptical Galaxies. ESO, Garching, p. 225

Bacon R., 1985, A&A, 143, 84

Bender R., 1988, A&A, 193, L7

Bender R., 1990a, in Wielen R., ed., Dynamics and Interactions of Galaxies. Springer-Verlag, Berlin, p. 232

Bender R., 1990b, A&A, 229, 441
Bender R., Döbereiner S., Möllenhoff C., 1988, A&AS, 74, 385
Bertola F., Bettoni D., Danziger I. J., Sadler E., Sparke L., de Zeeuw P. T., 1991, ApJ, 373, 369
Bertola F., Pizzella A., Persic M., Salucci P., 1993, ApJ, 416, L45
Binney J. J., de Vaucouleurs G., 1981, MNRAS, 194, 679
Binney J. J., Tremaine S., 1987, Galactic Dynamics. Princeton Univ. Press, Princeton
Binney J., Davies R. L., Illingworth G. D., 1990, ApJ, 361, 78
Boroson T. A., 1981, ApJS, 46, 177
Bregman J. N., Hogg D. E., Roberts M. S., 1992, ApJ, 387, 484
Burstein D., 1979, ApJ, 234, 829
Buson L. M. et al., 1993, A&A, 280, 409
Caldwell N., 1984, ApJ, 278, 96
Caldwell N., Kirshner R. P., Richstone D. O., 1986, ApJ, 305, 136
Capaccioli M., 1987, in de Zeeuw P. T., ed., Proc. IAU Symp. 127, Structure and Dynamics of Elliptical Galaxies. Reidel, Dordrecht, p. 47
Capaccioli M., 1990, in Jarvis B. J., Terndrup D. M., eds, Bulges of Galaxies. ESO, Garching, p. 231
Capaccioli M., Caon N., 1992, in Longo G., Capaccioli M., Busarello G., eds, Morphological and Physical Classification of Galaxies. Kluwer, Dordrecht, p. 99
Carter D., 1987, ApJ, 312, 514
Cinzano P., van der Marel R. P., 1993, in Danziger I. J., Zeilinger W. W., Kjär K., eds, Structure, Dynamics and Chemical Evolution of Elliptical Galaxies. ESO, Garching, p. 105
Cuddeford P., Binney J. J., 1994, MNRAS, 266, 273
Davies R. L., Burstein D., Dressler A., Faber S. M., Lynden-Bell D., Terlevich R. J., Wegner G., 1987, ApJS, 64, 586
Dehnen W., Gerhard O. E., 1993, MNRAS, 261, 311
de Vaucouleurs G., de Vaucouleurs A., Corwin H. G. Jr, Buta R. J., Paturel H. G., Fouqué P., 1991, 3rd Reference Catalogue of Bright Galaxies. Springer-Verlag, New York (RC3)
de Zeeuw P. T., Franx M., Peletier R., 1986, MNRAS, 221, 1001
Disney M., Phillipps S., 1985, MNRAS, 216, 53
Djorgovski S., 1985, PhD thesis, Univ. California, Berkeley
Evans N. W., 1993, MNRAS, 260, 1991
Evans N. W., 1994, MNRAS, 267, 333
Evans N. W., Collett J. L., 1993, MNRAS, 264, 353
Fasano G., 1990, Rapporto Interno, Padova Astronomical Observatory
Fillmore J. A., Boroson T. A., Dressler A., 1986, ApJ, 302, 208
Franx M., Illingworth G. D., 1988, ApJ, 327, L55
Franx M., Illingworth G. D., Heckman T., 1989, ApJ, 344, 613
Freeman K. C., 1970, ApJ, 160, 811
Gerhard O. E., 1993, MNRAS, 265, 213
Governato F., Reduzzi L., Rampazzo R., 1993, MNRAS, 261, 379
Kent S. M., 1988, AJ, 96, 514
Kim D. W., 1989, ApJ, 346, 653
Kim D. W., Guhathakurta P., van Gorkom J. H., Jura M., Knapp G. R., 1988, ApJ, 330, 684
Kuijken K., Tremaine S., 1992, in Sundelius B., ed., Dynamics of Disc Galaxies. University of Göteborg Press, Göteborg, Sweden, p. 71
Landolt A. U., 1983, AJ, 88, 439
Lewis J. R., Freeman K. C., 1989, AJ, 97, 139
McElroy D. B., 1983, ApJ, 270, 485
Miyamoto M., Nagai R., 1975, PASJ, 27, 533
Moffat A. F. J., 1969, A&A, 3, 455
Nieto J. L., Poulain P., Davoust E., Rosenblatt P., 1991, A&AS, 88, 559
Peletier R. F., Davies R. L., Illingworth G. D., Davies L. E., Cawson M., 1990, AJ, 100, 1091
Rix H. W., White S. D. M., 1990, ApJ, 362, 52
Rix H. W., White S. D. M., 1992, MNRAS, 254, 389
Sandage A., Tammann G. A., 1981, A Revised Shapley-Ames Catalogue of Bright Galaxies. Carnegie Institution of Washington, Washington D.C. (RSA)
Scorza C., 1993a, in Danziger I. J., Zeilinger W. W., Kjär K., eds, Structure, Dynamics and Chemical Evolution of Elliptical Galaxies. ESO, Garching, p. 115
Scorza C., 1993b, PhD thesis, Landessternwarte Heidelberg, Germany
Scorza C., Bender R., 1990, A&A, 235, 49
Simien F., Michard R., 1984, in Nieto J. L., ed., New Aspects of Galaxy Photometry. Springer-Verlag, Berlin, p. 345
Stiavelli M., Londrillo P., Messina A., 1991, MNRAS, 251, 57P
Toomre A., 1964, ApJ, 139, 1217
van der Kruit P., Freeman K. C., 1986, ApJ, 303, 556
van der Marel R. P., 1991, MNRAS, 253, 710
van der Marel R. P., Cinzano P., 1992, in Longo G., Capaccioli M., Busarello G., eds, Morphological and Physical Classification of Galaxies. Kluwer, Dordrecht, p. 437
van der Marel R. P., Franx M., 1993, ApJ, 407, 525 (vdMF)
van der Marel R. P., Binney J. J., Davies R. L., 1990, MNRAS, 245, 582
van der Marel R. P., Rix H. W., Carter D., Franx M., White S. D. M., de Zeeuw P. T., 1994a, MNRAS, 268, 521
van der Marel R. P., Evans N. W., Rix H. W., White S. D. M., de Zeeuw P. T., 1994b, MNRAS, in press